

# Geometrical determinant of nonlinear synaptic integration in human cortical pyramidal neurons

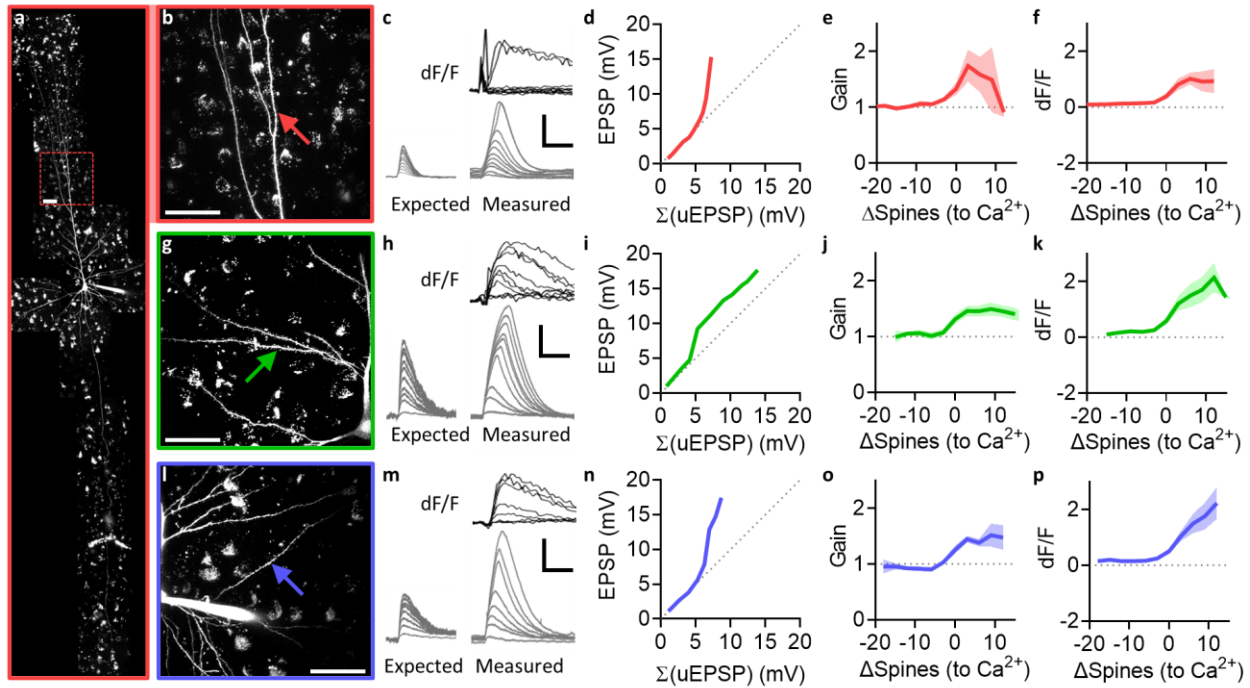
Jaeyoung Yoon<sup>1,2,\*</sup>, et al.<sup>†</sup>

<sup>1</sup> McGovern Institute for Brain Research, Massachusetts Institute of Technology, Cambridge, MA 02139, USA.

<sup>2</sup> Present address: F. M. Kirby Neurobiology Center, Boston Children's Hospital, & Harvard Medical School, Boston, MA 02115, USA.

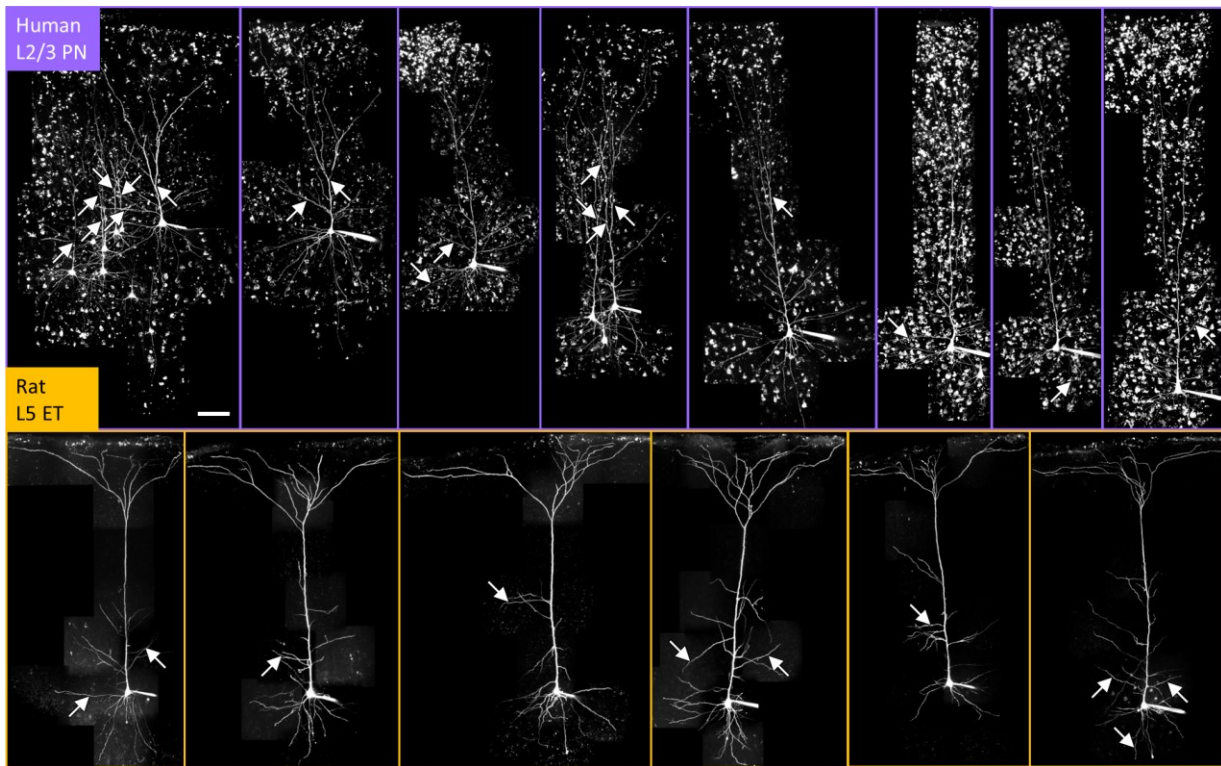
\* Correspondence: jy.yoon@tch.harvard.edu

<sup>†</sup> Full author list to be determined



12

**Figure 1.** Synaptic integration at human neocortical layer 2/3 pyramidal neurons (L2/3 PN). **(a)** Representative example of an L2/3 PN. Scale bar, 50  $\mu\text{m}$ . **(b)** Same cell as in panel **a**, at the apical tuft. Arrow indicates the center of synaptic spine clusters that were activated by 2-photon glutamate uncaging (2PGU), which typically spanned approximately 30-40  $\mu\text{m}$  along the length of the branch. **(c)** Representative examples of expected EPSP (left), calculated from the arithmetic sum of unitary EPSP (uEPSP) recorded from each spine, and measured EPSP (right, bottom) recorded by quasi-simultaneous activation of spines shown in panel **b**, along with associated dF/F traces (right, top) obtained by intracellular calcium imaging. Scale bars, 50 ms, 5 mV, 1.0 dF/F. **(d)** Representative example of measured EPSP, plotted against the arithmetic sum of uEPSPs, from the activation of the same spines as shown in panels **b-c**. **(e)** Grouped average from all apical tuft dendrites ( $n = 24$ ). Gain is defined by the ratio of measured vs. expected EPSP, or the measured EPSP divided by the sum of corresponding uEPSPs. The number of activated spines are aligned to the threshold at which  $\text{Ca}^{2+}$  signal was first observed. **(f)** Grouped average of dF/F, associated with data shown in panel **e**. **(g-k)** Similar to panels **b-f**, but from oblique dendrites ( $n = 16$ ) branching from the apical trunk. **(l-p)** Similar to panels **b-f** or **g-k**, but from basal dendrites ( $n = 20$ ) branching from the soma.



30

31 **Figure 2.** Representative examples showing the location of synaptic spines activated by 2PGU. For  
 32 simplicity, arrows indicate the center of the spine clusters. Top, human L2/3 PN; the high  
 33 background in human cortical images is caused by lipofuscin aggregates on the somata of neurons.  
 34 Bottom, rat L5 extratelencephalic (ET) cells. Scale bar, 100  $\mu$ m.

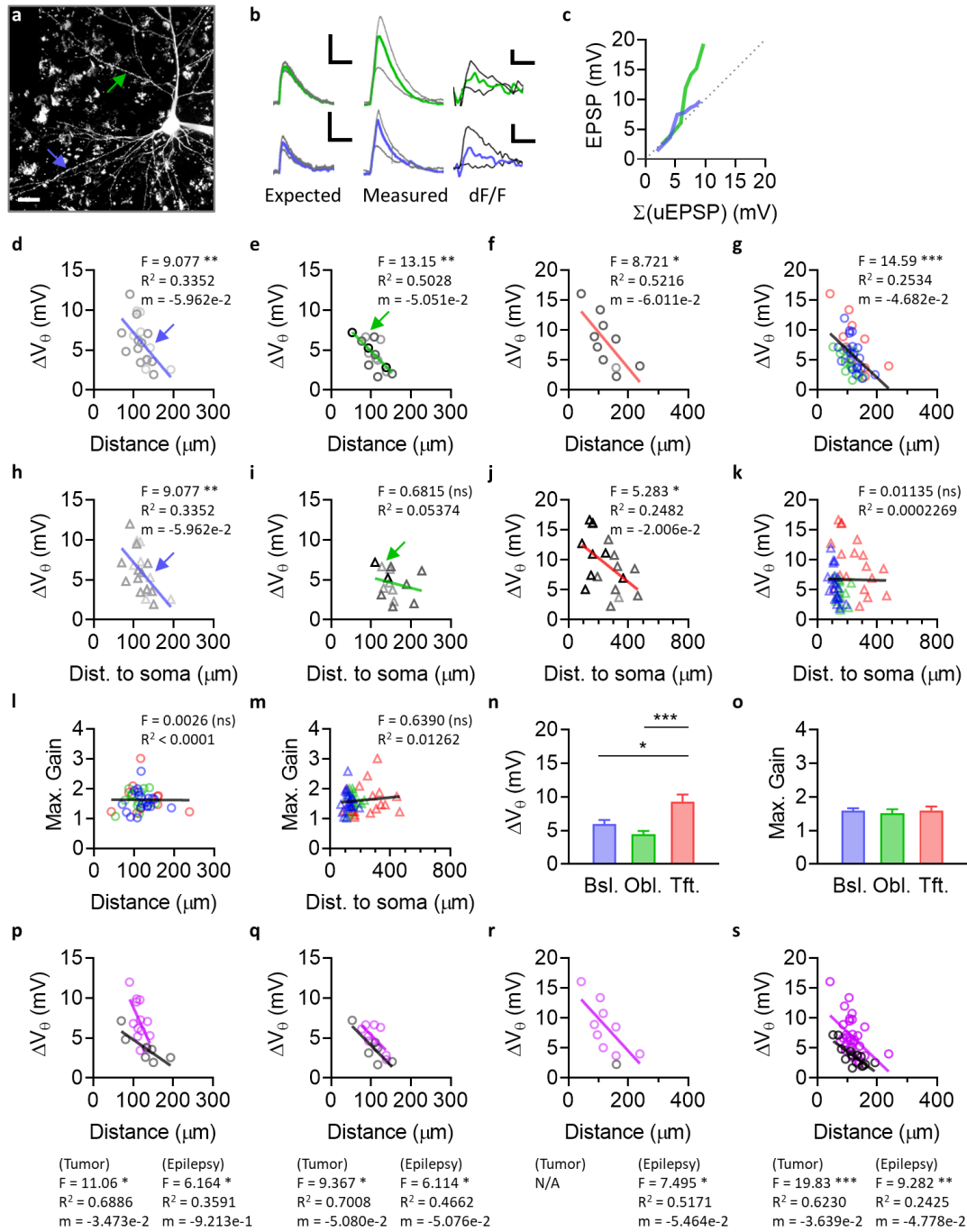


**Figure 3.** Somatic threshold potential at supralinearity is determined by the distance between the synaptic spines and the primary structure of human cortical neurons. **(a)** Representative example of a human L2/3 PN. Two different uncaging locations, one on a basal dendrite (blue) and another on an oblique dendrite (green), are indicated by arrows. Scale bar, 50  $\mu\text{m}$ . **(b)** Representative traces of expected and measured EPSP, along with associated dF/F, from the branches shown in panel **a**. Scale bars, 50 ms, 5 mV, 0.5 (bottom) or 0.1 (top) dF/F. **(c)** Measured EPSP vs. expected

43 EPSP from uEPSP sum, from the same branches shown in panels **a-b**. **(d-g)** Somatic nonlinearity  
44 threshold potential ( $\Delta V_{\theta}$ ), plotted against the curvilinear projected distance to primary structure.  
45  $\Delta V_{\theta}$  was defined by the somatic uEPSP sum at local nonlinearity threshold indicated by local  $\text{Ca}^{2+}$   
46 signal. The primary structure was defined as the soma and its immediate extension along the  
47 apical trunk up to any branch point. For  $\Delta V_{\theta}$ , expected EPSP from uEPSP sum was used instead of  
48 the actual measured EPSP to determine the accurate threshold irrespective of the nonlinear gain.  
49 **(d)**  $\Delta V_{\theta}$  at basal dendrites vs. distance to primary structure (soma). Different shades of symbols  
50 indicate increasing branch order (1<sup>st</sup> to 4<sup>th</sup>, darker to lighter, throughout panels **d-f**). **(e)**  $\Delta V_{\theta}$  at  
51 oblique dendrites vs. distance to primary structure (branch point at the apical trunk). **(f)**  $\Delta V_{\theta}$  at  
52 apical tuft dendrites vs. distance to primary structure (branch point at the apical trunk, i.e. nexus).  
53 **(g)** Data shown in panels **d-f**, overlaid for comparison. **(h-k)** similar to panels **d-g**, but plotted  
54 against distance to soma instead of primary structure; note that by definition of primary structure,  
55 panel **h** is identical to panel **d**. **l**. Maximum gain vs. distance to primary structure. **m**. Maximum  
56 gain vs. distance to soma. **n**.  $\Delta V_{\theta}$  at basal, oblique, and tuft dendrites. **o**. Maximum gain at basal,  
57 oblique, and tuft dendrites. **(p-s)** Same data as in panels **d-g**, but grouped separately by tumor  
58 (black) or epilepsy (purple).

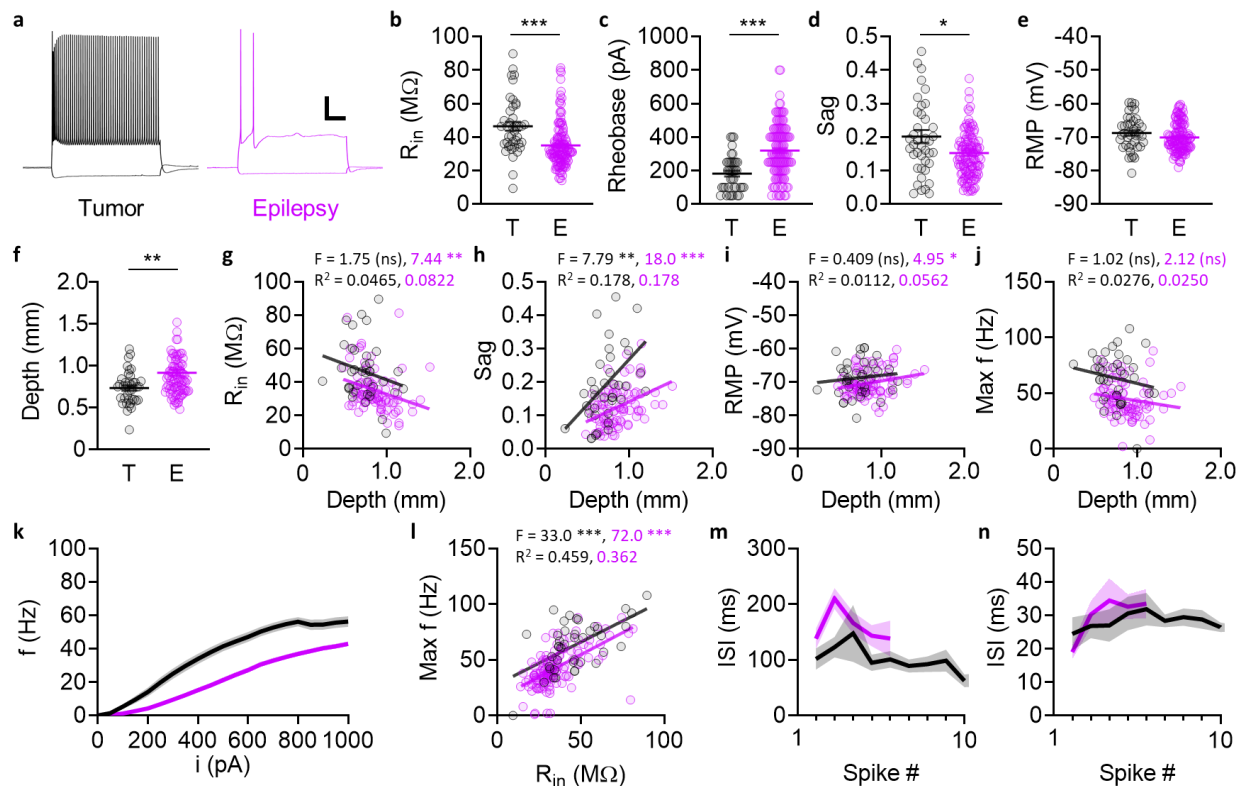
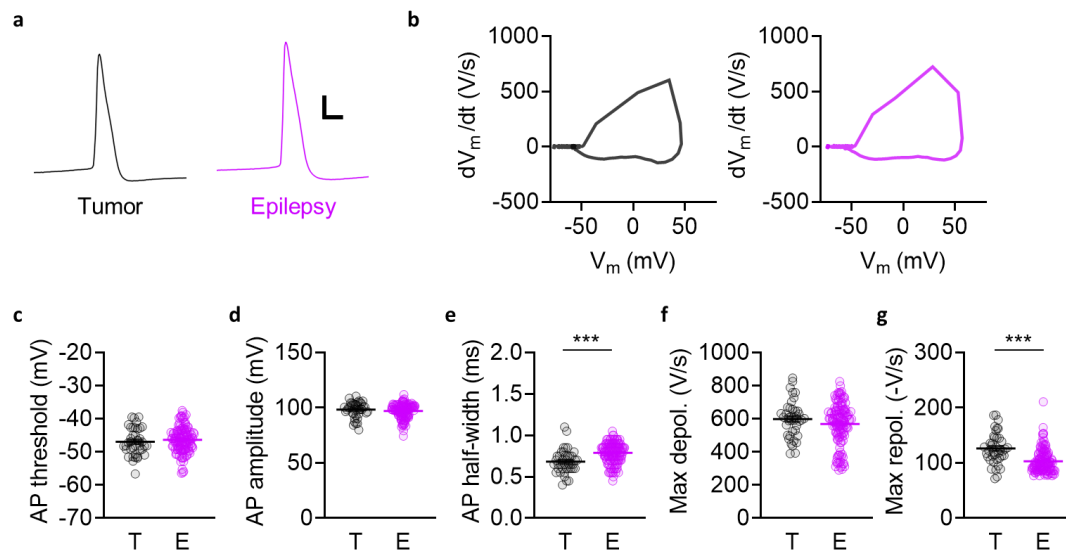


**Figure 4.** Intrinsic membrane properties of human L2/3 PN, from tumor (black) or epilepsy (purple). For more detailed patient and tissue information, see **Table 1**. Note that tissue from both tumor and epilepsy patients originated from areas determined to be nonpathological, but removed as part of the surgical procedure. **(a)** Representative traces of membrane potential responses to somatic step current injection (-250 pA, +1000 pA). Scale bar, 20 mV, 200 ms. The example to the right was taken from the same cell as in **Fig. 1a**. **(b)** Input resistance ( $R_{in}$ ). See methods for  $R_{in}$  calculation. **(c)** Rheobase, with current step resolution of 50 pA. **(d)** Sag ratio. See methods for the definition of sag ratio. **(e)** Resting membrane potential (RMP). **(f)** Sampling bias in the cortical depths of recorded L2/3 PN included in the current study. Cortical depth of a recorded cell was defined as the linear distance between the pial surface and the center of the mass of the somatic boundary, extrapolated from the line connecting the soma and the nexus. **(g-j)** Intrinsic membrane properties, plotted against cortical depth. **(g)**  $R_{in}$ . **(h)** Sag ratio. **(i)** RMP. **(j)** Peak firing rate. **(k)** Firing frequency in response to somatic current injection ( $f$ - $i$  curve). **(l)** Peak firing rate, plotted against  $R_{in}$ . **(m)** Inter-spike interval (ISI) at rheobase. **(n)** ISI at  $2 \times$  rheobase.

75



76

77 **Figure 5.** Single action potential (AP) kinetics of human L2/3 PN, from tumor (black) or epilepsy  
 78 (purple). **(a)** Representative traces. For each cell, the first action potential generated at rheobase  
 79 was taken for analysis. Scale bar, 20 mV, 1 ms. The example to the right was taken from the same  
 80 cell as in **Fig. 3a**. **(b)** Example AP waveforms presented as  $dV/dt$  plots, calculated from the same  
 81 traces as in panel **a**. **(c)** AP threshold. AP threshold was defined as the  $V_m$  at which  $dV/dt$  crossed  
 82 10 (V/s). **(d)** AP amplitude (RMP to AP peak). **(e)** AP half-width. **(f)** Maximum rate of depolarization.  
 83 **(g)** Maximum rate of repolarization.

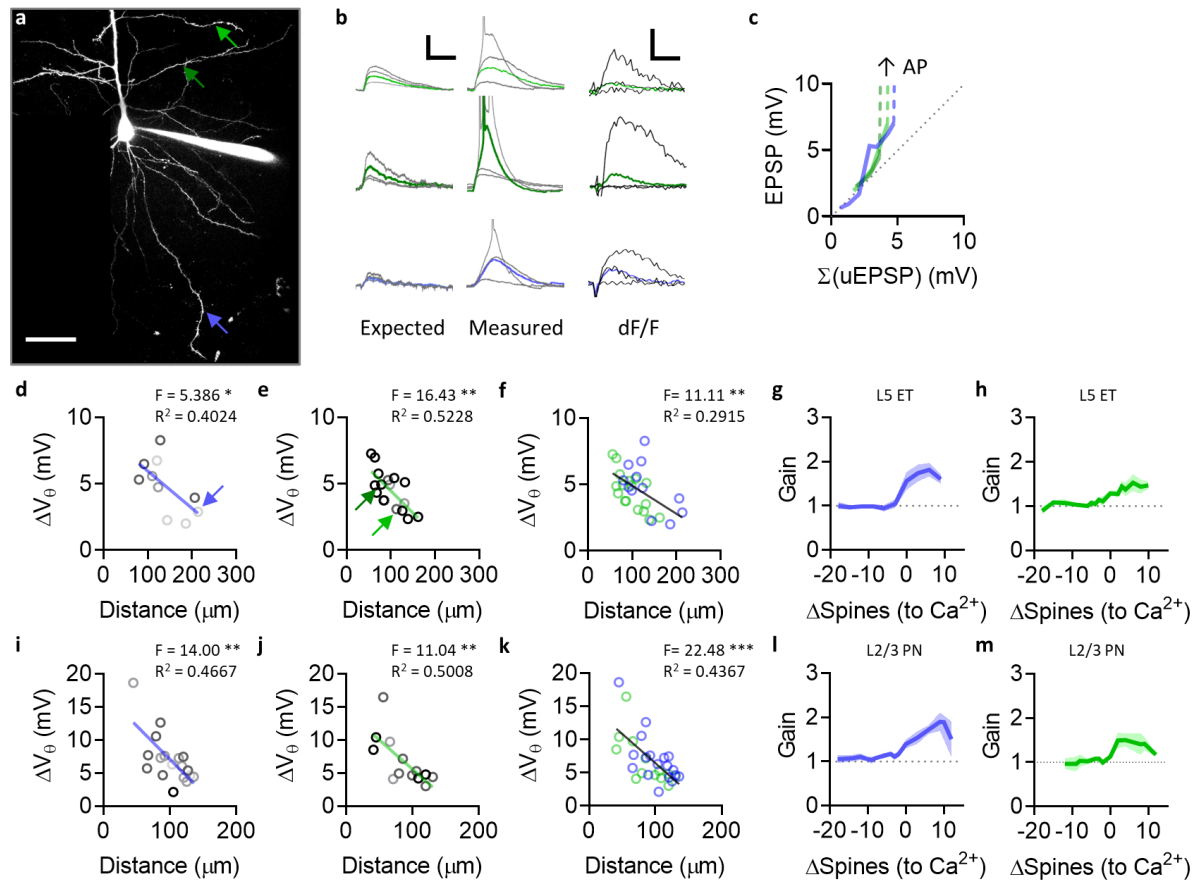


**Figure 6.** Somatic threshold potential at supralinearity is linearly correlated to synapse distance from primary structure in rodents as well as in humans, for both supragranular and infragranular rodent cortical pyramidal neurons. **(a)** Representative example of a rat L5 ET PN, from the temporal association area (TeA). Three different uncaging locations, one on a basal dendrite and two on separate oblique dendrites, are indicated by arrows. Scale bar, 50  $\mu\text{m}$ . **(b)** Representative traces from the uncaging locations shown in panel (a). Scale bars, 50 ms, 5 mV, 0.5 dF/F. **(c)** Measured EPSP vs. expected EPSP from uEPSP sum, from the branches shown in panels (a-b). **(d-f)**  $\Delta V_{\theta}$  vs. distance to primary structure, in rat L5 ET. **(d)** Basal dendrites. **(e)** Oblique dendrites. **(f)** Data shown in panels (d-e), overlaid for comparison. **(g)** Synaptic gain, at basal dendrites shown in panel (d). **(h)** Synaptic gain, at oblique dendrites shown in panel (e). **(i-m)** Similar to panels (d-h), but from rat L2/3 PNs instead of L5 ET. **(i)** Basal dendrites. **(j)** Oblique dendrites. **(k)** Data shown in panels (i-j), overlaid for comparison. **(l)** Synaptic gain, at basal dendrites shown in panel (i). **(m)** Synaptic gain, at oblique dendrites shown in panel (j).



ID	Age	Sex	Area	Hemi.	Medications (AED)	Diagnosis	n (cells/humans)
BA14	-	-	ATL	-	-	Epilepsy	6
BA27	-	-	TL	-	-	Epilepsy	6
BB05	22	M	FL	-	-	Epilepsy	1
BF30	34	F	TL	-	-	Epilepsy	1
BI30	-	-	TL	-	-	Epilepsy	3
BJ04	-	-	TL	-	-	Epilepsy	3
BJ06	-	-	FL	-	-	Epilepsy	1
BK02	55	M	ATL	R	Le	Tumor	10
BK05	32	M	TL	L	Cb, Le, O, T	Epilepsy	2
BK10	71	F	TL	R	-	Tumor	13
BK18	46	M	FL	L	Ce, O, Ph	Epilepsy	7
BL06	71	M	TL	R	-	Epilepsy	13
CC07	33	M	FL	R	B, Lc, Lo	Epilepsy	12
CC17	23	F	ATL	R	Cn, G, Lm, Le, Lo, T, Z	Epilepsy	43*
CC31	24	M	ATL	R	Lc, Le, O, T	Epilepsy	1
CG05	18	F	TL	R	Cb, G, Lm, Le, O, T	Epilepsy	6
CH15	57	F	TL	R	Le	Tumor	9
CH16	24	M	TL	R	E, G, Lm, Le, O, Pe	Epilepsy	16
CI08	30	M	TL	L	Lm, Le	Epilepsy	1
DA31	72	F	TL	R	-	Tumor	4
DB16	31	M	TL	R	-	Epilepsy	7
DC15	71	M	TL	R	-	Tumor	7
						(Tumor)	43/5
						(Epilepsy)	119/17
						(Total)	162/22

**Abbreviations:**

B, brivaracetam; Ce, cenobamate; Cb, clobazam; Cn, clonazepam; E, eslicarbazepine; G, gabapentin; Lc, lacosamide; Lm, lamotrigine; Le, levetiracetam; Lo, lorazepam; O, oxcarbazepine; Pe, perampanel; Ph, phenytoin; T, topiramate; Z, zonisamide; -, not available (not applicable or unknown). Note that only limited information was made available for a subset of cases (n = 21/7, from a total of 162/22 (cells/humans)).

\* Recorded up to 120 h post-resection (typically 24 to 48 h)

## Methods

### *Brain slice preparation*

For human brain slices, resected tissue was immediately placed in an ice-cold solution at the operating theater. The cutting solution used for transport and slicing contained (in mM): 165 sucrose, 20 HEPES, 25 NaHCO<sub>3</sub>, 2.5 KCl, 1.25 NaH<sub>2</sub>PO<sub>4</sub>, 20 D-glucose, 5 Na-ascorbate, 3 Na-pyruvate, 0.5 CaCl<sub>2</sub>, 7 MgCl<sub>2</sub>, pH adjusted to 7.3, 300-310 mOsm. All compounds were obtained from Sigma Aldrich unless otherwise specified. The tissue container was kept in a thermally isolated transportation box filled with ice packs and transported from the operating room at Massachusetts General Hospital (MGH) or Brigham and Women's Hospital (BWH) to the laboratory at Massachusetts Institute of Technology (MIT) within 25 minutes. The tissue block was then placed orthogonal to the pia to preserve cortical layers and white matter in proper orientation. Slices of 300  $\mu$ m thickness were prepared with a vibratome (VT1200S, Leica), and maintained at 36 °C for at least 1 hour in the recovery solution containing (in mM): 90 NaCl, 20 HEPES, 25 NaHCO<sub>3</sub>, 2.5 KCl, 1.25 NaH<sub>2</sub>PO<sub>4</sub>, 20 D-glucose, 5 Na-ascorbate, 3 Na-pyruvate, 1 CaCl<sub>2</sub>, 4 MgCl<sub>2</sub>, pH adjusted to 7.3, 300-310 mOsm. All solutions were continuously aerated with carbogen (95% O<sub>2</sub> / 5% CO<sub>2</sub>) throughout the course of experiments, including transport and slicing, and refreshed every 6-8 hours. Experiments were performed typically within a period of 24 or 48 hours following resection, with exception (see Table 1). For rodent brain slices, 12-week-old animals were anesthetized with isoflurane prior to decapitation; the cutting solution contained (in mM): 225 sucrose, 25 NaHCO<sub>3</sub>, 2.5 KCl, 1.25 NaH<sub>2</sub>PO<sub>4</sub>, 20 D-glucose, 0.5 CaCl<sub>2</sub>, 7 MgCl<sub>2</sub>, 300-310 mOsm, and slices were recovered in artificial cerebrospinal fluid (aCSF) identical to the recording solution. All protocols were approved by the internal review board (IRB) and/or the institutional animal care and use committee (IACUC) at the respective institution(s).

### *Whole-cell patch clamp*

All experiments were conducted under identical conditions. Slices were placed in a recording chamber and visualized with Dodt gradient contrast microscopy (Examiner Z1, Zeiss), while being perfused with the recording aCSF at a flow rate of 1.6 mL/min using a peristaltic pump (Minipuls 3, Gilson). The recording solution contained (in mM): 125 NaCl, 25 NaHCO<sub>3</sub>, 3 KCl, 1.25 NaH<sub>2</sub>PO<sub>4</sub>, 10 D-glucose, 1.2 CaCl<sub>2</sub>, 1.2 MgCl<sub>2</sub>, 300-310 mOsm, maintained at 36 °C with an inline heating system (TC344C & SH28, Warner). Recordings were made from the soma of pyramidal neurons (PN) in layer 2/3 (L2/3) of the human neocortex, or L2/3 and L5 of the rat temporal association area (TeA), using a MultiClamp 700B amplifier (Molecular Devices). Data were Bessel filtered at a cutoff frequency of 10 kHz and acquired at a sampling rate of 20 kHz, digitized and recorded with Prairie View (Bruker), and analyzed with PVBS (<https://github.com/flosfor/pvbs>). Patch pipettes (2.5-4.0 M $\Omega$ ) were pulled from borosilicate glass capillaries (PG52151-4, WPI) with a horizontal pipette puller (P-1000, Sutter), and positioned using a set of micromanipulators (Junior, Luigs & Neumann). The internal solution contained (in mM): 130 K-gluconate, 4 KCl, 4 NaCl, 10 HEPES, 15 phosphocreatine-di(tris), 4 Mg-ATP, 0.3 Na<sub>2</sub>-GTP, adjusted to pH 7.3 with KOH (typically 6-8 mM).

of additional  $K^+$  from KOH), 300-310 mOsm, with 0.05 mM Alexa Fluor 594 and 0.1 mM Oregon Green BAPTA-1 (Thermo Fisher) added for structural and calcium imaging. Pipette capacitance ( $C_p$ ) was fully compensated, typically  $\sim 13$ -14 pF. Series resistance ( $R_s$ ) was continuously monitored throughout the course of recordings, and cells with  $R_s \leq 20$  M $\Omega$  with less than 15% change were accepted. To measure the intrinsic neuronal membrane properties, cells were held in current clamp at 0 pA, and injected at the soma with current steps (-250 to +1000 pA at 50 pA steps, 500 or 1000 ms duration), with bridge fully balanced.  $R_{in}$  was calculated from the linear fit crossing the origin obtained from the transient membrane potential responses to step current input to minimize the contribution from hyperpolarization-activated current ( $i_h$ ). Sag ratio was defined as the difference between the transient and steady-state voltage response, divided by the transient voltage response in alignment with the definition of  $R_{in}$ . For action potential (AP) waveform analysis, the first AP generated at rheobase was used. AP threshold was defined as the membrane potential immediately preceding the point at which  $dV/dt$  first exceeded 10 (V/s). AP amplitude was calculated as the difference between the AP peak and AP threshold, and the width at half of this amplitude was taken as AP half-width. Liquid junction potential, which was measured at  $\sim 11$ -12 mV, was not corrected for in the membrane potential values reported in the current study.

### *2-photon glutamate uncaging and calcium imaging*

All experiments were conducted at the 2-photon core facility (46-6178) at the McGovern Institute for Brain Research (MIBR), MIT. 2-photon excitation microscopy (2PEF) for simultaneous structural imaging, glutamate uncaging (2PGU), and calcium imaging was performed using two Ti:sapphire lasers (Mai Tai eHPDS, Spectra Physics), modulated and guided with a custom-built optical setup including electro-optic modulators (M350-80, Conoptics) and an 8x pulse splitter ([https://flosfor.github.io/pulse\\_splitter.pdf](https://flosfor.github.io/pulse_splitter.pdf)). Optical elements in the excitation and emission pathways were obtained from Thorlabs or Chroma, unless otherwise specified. Emission signals were acquired with two photomultiplier tubes (H7422-40, Hamamatsu), after wavelength separation. For structural and calcium imaging, cells were visualized with Alexa Fluor 594 and Oregon Green BAPTA-1 included in the internal solution as described above, respectively excited with 880 nm or 920 nm. For calcium imaging, line scans (256 repetitions of  $\sim 10$   $\mu$ m lines, each with  $\sim 1$  ms duration at 8.25  $\mu$ s resolution) were made across the dendritic branch, near the center of the synaptic spines activated with 2PGU. The region of interest (ROI) and background for  $dF/F$  calculation were defined respectively as those regions with signal intensities above the 2<sup>nd</sup> percentile or below the 50<sup>th</sup> percentile during the baseline period prior to 2PGU pulse delivery. For 2PGU, 5 mM MNI-caged-L-glutamate (Tocris) was dissolved in recording aCSF (adjusted to 120 mM NaCl to compensate for osmolarity), and delivered with a puffer pipette of pore size  $\sim 15$ -20  $\mu$ m in diameter, positioned  $\sim 100$   $\mu$ m away from the synaptic spines at a vertical angle of 20 degrees. 2PGU was achieved with 720 nm excitation, quasi-simultaneously at an interval of 0.12 ms between each spine with a dual galvanometer scanner (Bruker), at an intensity producing physiological uEPSP amplitudes typically at  $\sim 0.1$  to 0.5 mV (or corresponding to  $\sim 50$  to 100 mW when measured with continuous full-field illumination, instead of short, focalized pulses used for actual experiments),  $\sim 0.1$   $\mu$ m from the head of each dendritic spine. A total of 20-35 spines, typically spanning  $\sim 30$ -40  $\mu$ m along the length of the dendrite, were activated at a given branch.

183

184 *Data analysis*

185 Electrophysiology and calcium imaging data were analyzed and visualized using PVBS  
186 (<https://github.com/flosfor/pvbs>). Structural imaging data were processed with imageJ  
187 (<https://imagej.net>). Plots were made using custom codes written in MATLAB (Mathworks), and  
188 Prism (GraphPad). Statistical information is expressed as mean  $\pm$  standard error of the mean  
189 (SEM), where n indicates the number of branches or cells, as applicable. Statistical significance  
190 was accepted when  $P < 0.05$  (\*  $P < 0.05$ ; \*\*  $P < 0.01$ ; \*\*\*  $P < 0.001$ ) with Mann-Whitney U test,  
191 unless otherwise specified.

192

193

194 **Acknowledgements**

195 We thank the clinical and research coordination personnel at MGH and BWH for the availability  
196 of human brain tissue for research. This work was supported by the Y. Eva Tan Postdoctoral  
197 Fellowship from the Yang-Tan Center for Molecular Therapeutics in Neuroscience at MIT.

198

199